Mohsenian, V., Filizadeh, R., Hajirasouliha, I. and Garcia, R. (2020) Seismic performance assessment of eccentrically braced steel frames with energy-absorbing links under sequential earthquakes. Journal of Building Engineering, p.101576. https://doi.org/10.1016/j.jobe.2020.101576

Seismic Performance Assessment of Eccentrically Braced Steel Frames with Energy-Absorbing Links under Sequential Earthquakes

Vahid Mohsenian[a], Reza Filizadeh[b], Iman Hajirasouliha[c*], Reyes Garcia[d]

[a] *Department of Civil Engineering, University of Science and Culture, Tehran, Iran*

[b] *Department of Civil Engineering, Sharif University of Technology, Tehran, Iran*

[c] *Department of Civil and Structural Engineering, The University of Sheffield, Sheffield, UK*

[d] *School of Engineering, The University of Warwick, Coventry, UK*

* Corresponding author. Email: i.hajirasouliha@sheffield.ac.uk

Abstract: Recent studies have indicated the need of considering aftershocks in the seismic design/assessment of structures. This article investigates the effect of sequential mainshock and aftershock earthquakes on eccentrically braced steel framed with vertical energy-absorbing links. To achieve this, 4, 8 and 12 storey frame buildings are modelled in Perform3D® software considering non-linear behaviour of materials and components. The frames are subjected to a set of 12 main earthquake records corresponding to the required hazard level, and then subsequent aftershocks are applied using incremental dynamic analysis (IDA). To reduce the computational cost, an alternative approach is also adopted by applying the main earthquakes to the system followed by pushover analyses on the damaged building assuming a lateral load distribution proportional to the shape of the first vibration mode. Subsequently, the fragility curves are obtained for different damage levels, before and after the main earthquake. The results show that the eccentric braced frames with vertical links subjected to sequential earthquakes comply well with the performance levels of the Iranian Seismic Code. This study contributes towards the assessment and seismic validation of structures with eccentrically braced steel framed with vertical energy-absorbing links to sequential earthquakes.

Keywords: Eccentric Braced Frames; Vertical Link; Aftershocks; Sequential Earthquakes; Incremental Dynamic Analysis.

1. Introduction

After strong earthquakes, numerous aftershocks typically occur even after months of the main event (e.g. Maule in Chile, 2010; Van in Turkey, 2011; Ahar City in Iran, 2012). Whilst the magnitude of most aftershocks is lower than that of the main event, they can produce additional damage to buildings damaged during the main earthquake. Aftershocks can even lead to structural collapse of buildings, as reported in recent strong earthquakes (Zare, 2015; IIEES, 2019).

Previous research has investigated extensively the effect of aftershocks on steel frame structures. For instance, Lee and Foutch (2004) analysed the behaviour of steel frames under

successive artificial records. Whilst the damage produced by the first earthquake did not jeopardise the overall stability of the analysed structures, the application of the same earthquake (as an aftershock) to the damaged structure led to its collapse. However, it has been reported that the use of the main earthquake as an aftershock can over-estimate displacement demands. Fragiacomo et al. (2004) applied sequences of seismic records on elasto–plastic single-degree-of-freedom (SDOF) systems, moment resistant frames, and concentrically braced steel frames to propose suitable reduction factors for design. Li and Ellinwood (2007) developed an analytical tool for analysing the stochastic structural response of steel frames to sequences of earthquake ground motion. Loulelis et al. (2012) carried out parametric analyses on 36 moment-resisting steel frames using real and artificial seismic sequences. They provided practical empirical expressions to calculate damage and the behaviour factor of steel frames subjected to sequential ground motions. Song et al. (2014) and Li et al. (2014) evaluated the effect of frequency content and the duration of aftershocks on the probability of collapse of steel frames. The results indicated that long and low-frequency aftershocks were more destructive on buildings damaged during the main earthquake.

Ruiz-Garcia and Aguilar (2017) studied the influence of the modelling parameters in the response of a steel frame subjected to sequential earthquakes. The results confirmed the importance of selecting an appropriate modelling approach for the structure, as well as the need of including explicitly the post-mainshock residual drifts to assess the seismic behaviour of buildings under aftershocks. Guerrero et al. (2017) subjected steel buildings with Buckling-Restrained Braces to seismic sequences typical of soft soils. In their study, Guerrero et al. provided a series of design equations to calculate the peak and residual inter-storey drift demands under mainshocks and the sequence mainshock-aftershock events. In a subsequent study, Ruiz-Garcia et al. (2018a) investigated the seismic behaviour of eccentrically braced steel frames. Their results indicate that strong aftershocks could increase inter-storey drift demands once the shear links failed, and that the links' adjacent elements (beams and columns) could exhibit inelastic behaviour. More recent research by Ruiz-Garcia et al. (2018b) has also suggested that the behaviour of 3D modelled buildings can be different to that of 2D counterparts. Overall, the results from previous studies indicate that aftershocks increase the ductility demand, amount of damage and damage sequence of structures. Whilst there is evidence that aftershocks affect negatively the behaviour of structures, the effect of aftershocks on seismic design of structures is not included in current design codes (Hatzigeorgiou and Liolios, 2010; Hatzigeorgiou and Beskos, 2009; Ruiz-García and Negrete-Manriquez, 2011; Ruiz-García, 2012).

Silwal et al. (2018) reported that the use of superelastic viscous dampers in steel moment-frames subjected to seismic sequences improved the aftershock capacity of such structures. Park et al. (2018) proposed a methodology to calculate the fragility of damaged steel structures subjected to aftershocks. One of the main advantages of their methodology is that it can be used to choose sequences to which a structure can be vulnerable after the occurrence of a mainshock. By performing fragility analyses on of Buckling-Restrained Braced Frames, Veismoradi et al. (2018) indicated that the probability of exceedance of damage states increased by up to 1.5 times when this type of frame was subjected to seismic sequences. In one of the very few experimental studies in the literature, Rad et al. (2019) carried out shake table tests on a 1/2-scale two-storey steel frame to assess the effectiveness of different 'straightening' techniques at reducing residual drifts during aftershocks. Abdollahzadeh et al. (2019) proposed a modified Performance-based Plastic Design method able to control drift ratios and plastic hinge formation in steel frames under mainshock-aftershock sequences. Khatami et al. (2019) examined pounding effects on

steel moment-resisting frames with a soft storey at the ground floor. For the case studies examined, the separation gap required between buildings subjected to seismic sequences was up to 35% wider than that required for a singular earthquake. More recently, Shi et al. (2020) proposed probabilistic seismic demand models and hazard curves for steel frames with or without shape memory alloy bracing systems under mainshock-aftershock sequences. As found in previous studies, Parekar and Datta (2020) confirmed that height-wise stiffness irregularity in steel moment-resisting frames subjected to aftershocks led to an increase in interstorey drift demands.

In general, the previous studies discussed above have adopted four approaches for analysis of structures subjected to aftershocks:

1. Real seismic records including main earthquake and recorded aftershocks: whilst this method is probably the most suitable, issues such as easy access to real records, incompatibility of fault mechanisms and different soil conditions limit its applicability.

2. Back-to-back method: after the main earthquake, aftershocks are applied to the structure using the same record. However, in reality it is unlikely that an earthquake of exactly the same characteristics occurs sequentially at the same location.

3. Back-to-back coefficient method: in this method the aftershock is obtained by multiplying the main event by a coefficient that depends on the maximum acceleration, magnitude and distance from the fault of the earthquake. However, the fundamental frequency of the earthquake and the aftershocks are the same, which is a main drawback.

4. Randomised method: in this case artificial sequences are obtained by choosing a mainshock earthquake event followed by a randomly selected aftershock from a set of preselected real mainshocks.

To bypass the complexity of selecting a suitable aftershock, Luco et al. (2004) proposed an alternative approach where the residual capacity against collapse of a mainshock-damaged building was calculated by performing static (pushover) analyses on the building. Subsequent studies used a similar methodology (framework) to assess the response of post-mainshock building models under aftershocks of increasing seismic intensity (Jeon et al., 2015; Raghunandan et al., 2015; Ruiz-García and Aguilar, 2015; Burton et al., 2017; Veismoradia et al., 2018), with satisfactory results. With the availability of powerful computers, the above practical alternative methods can be easily implemented in commercial software for the assessment of buildings under sequential earthquakes.

In recent years, seismic links or “fuses” have been widely adopted in highly seismically active regions for the protection of buildings (e.g. Ghobarah and Elfath, 2001; Stratan and Dubina, 2002; Mazzolani et al., 2009; Della Corte et al., 2013; Mohsenian et al., 2020). The effectiveness of such “fuses” at improving the seismic behaviour of has been verified experimentally, as reported in the existing literature (Qu et al. 2018; Aghlara and Tahir, 2018; Yang et al., 2020; Jia et al., 2020).

The “fuses” are designed to deform well beyond their elastic limits, thus being able to sustain damage and dissipate large amounts of energy while the rest of the structure remains almost undamaged. If the fuse component experiences excessive damage, it can be replaced by a fraction of the cost compared to the total replacement cost of the structure. This article investigates the seismic performance of eccentrically braced steel frames with vertical energy-

absorbing links under mainshock and aftershock earthquake sequences. Such information is not currently available in literature and can help the wider application of this seismic resistant system is seismic regions. To achieve this, 4, 8 and 12 storey frame buildings are modelled in Perform3D® software considering non-linear behaviour of materials and components. The frames are then subjected to sequential earthquakes, and fragility curves are developed for different damage levels, before and after the main earthquake. To reduce the computational costs of conventional vulnerability assessment methods using incremental dynamic analysis (IDA), an alternative approach is also adopted by applying the original earthquake records corresponding to the required hazard level to the system followed by pushover analyses on the damaged building. This study contributes towards the assessment and seismic validation of structures with eccentrically braced steel framed with vertical energy-absorbing links subjected to sequential earthquakes.

2. Description of models and modelling assumptions

2.1 Geometry of buildings and initial design

4, 8 and 12-storey eccentrically braced steel frame buildings with three spans are analysed in this study (Figure 1). The storey height and span length are 3.2 m and 5 m, respectively, which represent typical dimensions of office buildings in the Middle East. The bracings and "fuse" link element (points B) are in the middle span. The office buildings are assumed to be located in a high seismic hazard area (design ground acceleration equal to 0.35g). Soil Type II ($375(m/s) \leq V_S \leq 750(m/s)$) is assumed as per the Iranian Seismic Code No. 2800 (2014), which is equivalent to soil Type C in ASCE/SEI 41-17 (2017). Permanent (Q_D) and live (Q_L) uniformly distributed loads are assumed along the beams (see Figure 1). A gravitational load $W=1.1[Q_D + 0.2Q_L]$ was used to combine lateral and vertical loads (see Figure 1). The gravitational load for all analysis (linear and nonlinear) was the same. The floors are assumed to behave as rigid diaphragms. In this study, all beams and columns are designed to comply with the Iranian Institute of National Building Regulations (2008) using ETABS® software (CSI, 2015). To calculate the seismic design loads, a response modification factor of 7 is adopted. Accordingly, the base shear coefficient of 0.125 for the 4 and 8 storey buildings, and 0.105 for the 12 storey building is obtained. Table 1 summarises the type and size of sections resulting from the design. The modulus of elasticity and Poisson's ratio of steel are assumed as 210 GPa and 0.3, respectively. It should be noted that in the adopted structural system, the brace elements with vertical links provide the lateral stability of the whole system and the other structural members are designed for gravity loads only. However, the yielding of vertical-links at one storey level does not necessarily lead to the failure of that storey, as the link elements can efficiently dissipate a major part of the earthquake input energy.

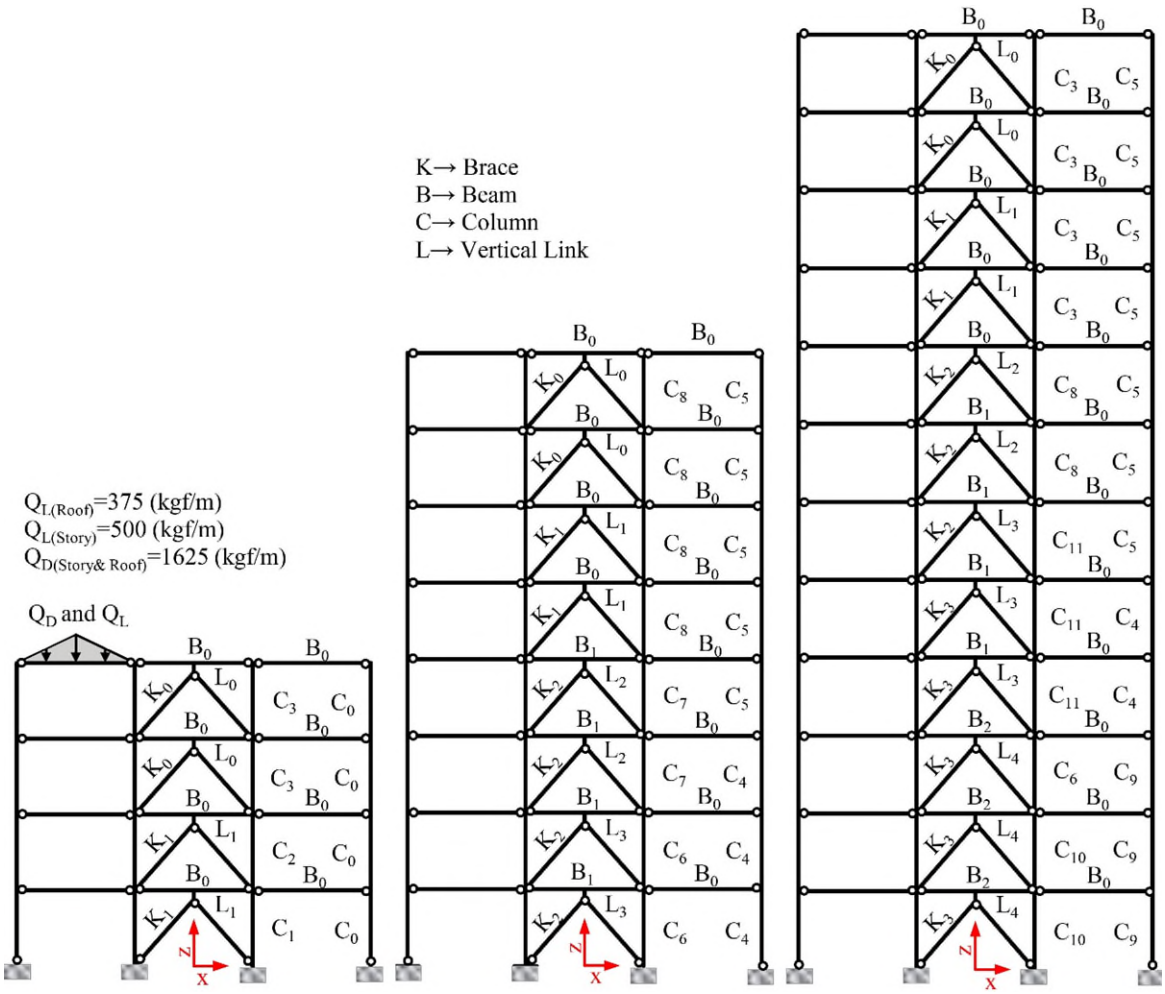

Figure 1. Geometry and loading used for the models

Table 1. Properties of the structural members (units: mm)

ID	Section	ID	Section	ID	Section	ID	Section
C_0	2IPE120	C_6	BOX(400×400×25)	K_0	2UPN100	B_2	IPE360
C_1	BOX(30×30×2.0)	C_7	BOX(350×350×15)	K_1	2UPN120	L_0	IPE160
C_2	BOX(250×250×10)	C_8	BOX(300×300×8)	K_2	2UPN140	L_1	IPE200
C_3	BOX(250×250×5)	C_9	2IPE180	K_3	2UPN160	L_2	IPE240
C_4	2IPE160	C_{10}	BOX(450×450×25)	B_0	IPE240	L_3	IPE270
C_5	2IPE140	C_{11}	BOX(350×350×10)	B_1	IPE300	L_4	IPE300

2.2 Modelling assumptions for nonlinear analyses

The buildings described in the previous section are modelled in PERFORM-3D software (CSI, 2016) to perform nonlinear analyses. In this study, all beam-to-column connections are assumed to be pinned connections as shown in Figures 1. Therefore, elastic elements are used to model the behaviour of beams at unbraced spans. Plastic hinges are assigned at the two ends of column elements at each storey level. The bracing elements are modelled following the ASCE/SEI 41-17 (2017) recommendations. For bracings with hinge connections that dissipate

energy through axial hinging, the axial deformation at the expected buckling load (Δ_c) and tensile load corresponding to the yield strength (Δ_t) can be taken as the ductility and nonlinear behaviour criteria, respectively. The axial deformation of the bracing is:

$$\Delta = FL / EA \qquad (1)$$

where F is the axial force; L is the free length of the bracing; A is its cross section area, and E is its modulus of elasticity.

In this study, the tensile and compressive behaviour of the bracings are modelled using the load-deformation curves shown in Figure 2a and b, respectively. The values (Δ_t) and (Δ_c) in these figures can be computed by replacing F in Equation 1 with the expected strength of the brace in tension (T_{CE}), and the lower bound of the strength under compression (P_{CL}). The parameters a, b and c in the figures are selected in accordance with ASCE/SEI 41-17 regulations.

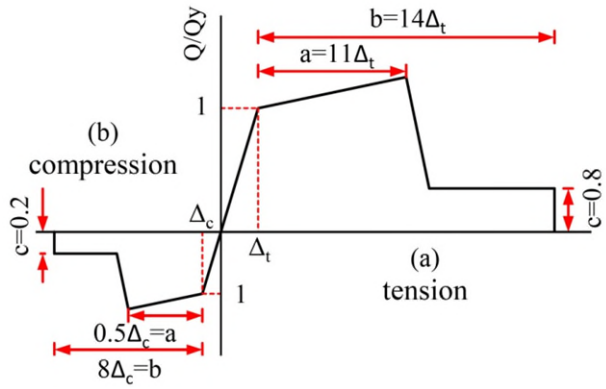

Figure 2. Load-deformation curve for brace elements, values 'a'=tension behaviour, and 'b'= compression behaviour (adopted from ASCE/SEI 41-17)

Figure 3 (a) shows schematically the deformation of the frame elements under lateral loading, whereas Figure 3 (b) illustrates the free diagram of beams and corresponding shear force and bending moment diagrams. Figure 3 indicates that, after the vertical links yield in shear, the axial force (F) and therefore the tensile and compressive deformation in the bracings (Δ_1 and Δ_2) remain constant. Consequently, upon yielding of the link, an increase in storey drift (Δs) would only increase the shear strains of the link itself. This behaviour is taken into account in the design of the bracing components.

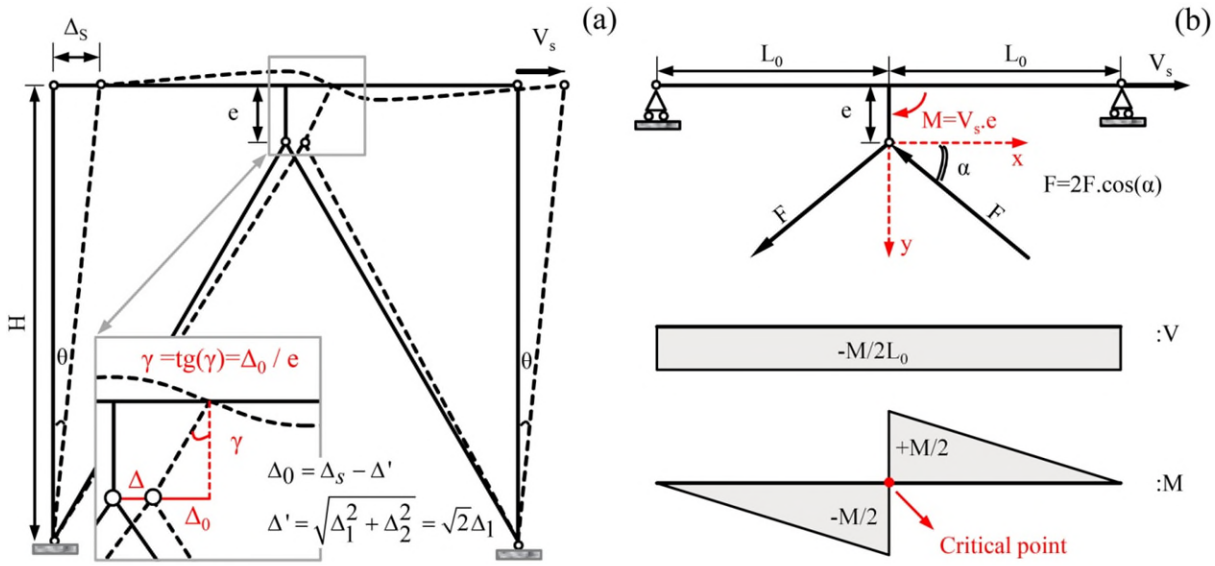

Figure 3. (a) Deformation of the frame elements under lateral displacement, and (b) free diagram of beams and shear force and bending moment diagrams

The beams in the braced spans are modelled as linear elements with lumped plasticity ("bending-rotational" and "shear" hinges) at the critical locations where they are connected to the vertical links (see Figure 3 (b)). The expected bending moment and shear capacities are calculated as $M_{CE}= Z.F_{ye}$ and $V_{CE}= 0.6F_{ye}.A_w$, respectively, where F_{ye} is the expected yield stress of steel ($F_{ye} =1.15F_y$ and $F_y =240$MPa), and A_w and Z are the plastic modulus and web area of the beam (ignoring the flange thickness).

The nonlinear behaviour of the vertical links is taken into account in the analyses and they are modelled to yield before the other elements to exhibit a "fuse" mechanism. The vertical links are fixed to the beam elements, while they are connected to the braces using pinned connections. The length of the links is chosen as 200 mm, as recommended by Sabouri-Ghomi and Saadati (2014) and Mohsenian and Mortezaei (2018, 2019), to ensure they exhibit shear yielding. After calculating MCE and VCE, the selected length of the elements (e= 200 mm) is compared to the ratio as recommended by ASCE/SEI 41-17 (2017) (see Table 2). The results indicate that the selected length would lead to shear yielding of the links at all storey levels ($e \le (1.6M_{CE}/V_{CE})$). The sections used for the link elements at different storey levels are given in Table 1 with the notations used in Figure 1. Table 2 also lists the actual length (e), ASCE/SEI 41-17 acceptance criteria ($1.6M_{CE}/V_{CE}$) and the normalised mechanical length of the link elements (eV_{CE}/M_{CE}).

The results indicate that all utilised link elements satisfy the acceptance criteria for shear controlled element according to ASCE/SEI 41-17 (2017). It should be noted that the study by Della Corte et al. (2013) showed that the tensile axial forces developed in shear link elements can increase their shear overstrength, especially for the shorter links with larger area of flanges. However, considering the opposite direction of the axial loads in the brace elements, the axial

loads in the vertical fuse links adopted in this study are negligible (please see Figure 3 (b)). Therefore, these effects can be considered to be negligible.

Table 2. Comparison between the length (e), ASCE/SEI 41-17 acceptance criteria ($1.6M_{CE}/V_{CE}$) and normalised mechanical length of the link elements (eV_{CE}/M_{CE})

Link section	e(mm)	$1.6M_{CE}/V_{CE}$	eV_{CE}/M_{CE}
IPE160	200	413.0	0.77
IPE200	200	526.2	0.61
IPE240	200	657.7	0.49
IPE270	200	724.3	0.44
IPE300	200	786.2	0.41

After designing the link sections as described above, the capacity and rotation angle of the links (γ) is computed using ABAQUS® (2014) by considering the interaction between shear force and bending moment (Bouwkamp et al. 2016,Vetr et al. 2017). Figure 4 shows the developed detailed FE model of the vertical link element. In this model, to simulate the shear behaviour, the bottom side of the element is considered to be fixed (connection to the beam), while the other side is free to rotate (connections to the braces).

The derived hysteresis curves are idealized as an equivalent multi-linear curve for use in the PERFORM-3D® (see Figure 5). It should be mentioned that the shear capacity of the sections obtained from this method (V_P) is generally in a good agreement with the results of equation $0.6F_{ye}.A_w$.

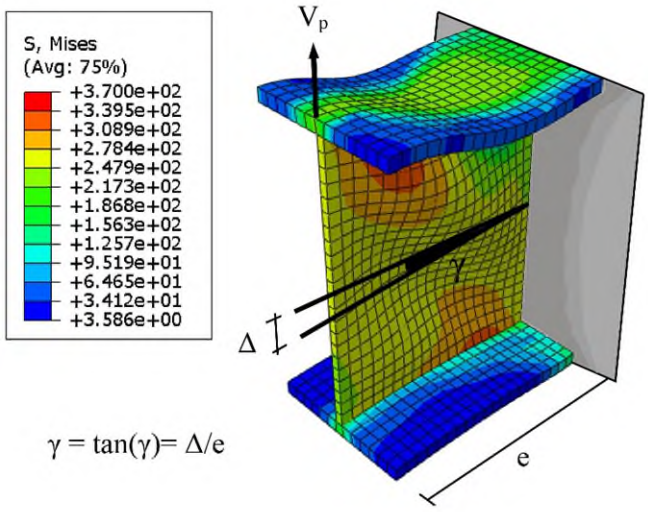

Damage States:			
(1)	(2)	(3)	(4)
$\gamma=\gamma_y=0.0024$(rad)	$\gamma=0.05$(rad)	$\gamma=0.08$(rad)	$\gamma=0.1$(rad)
$\sigma=F_y=240$ (MPa)	$F_y<\sigma<F_u$	$F_y<\sigma<F_u$	$\sigma=F_u=370$ (MPa)

Figure 4. Example of the deformations and maximum stresses in the links ($\gamma=0.1^{rad}$)

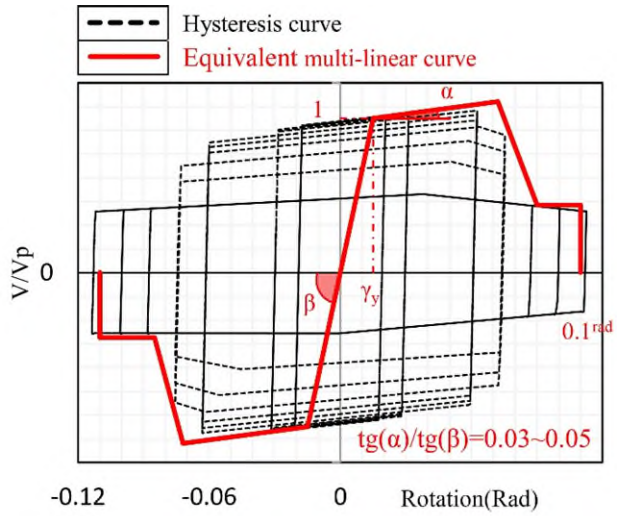

Figure. 5. A schematic example of the extracted hysteresis curve for the link element and the idealized multi-linear curves

In the present study, the shear deformation angle (γ) of the vertical links in the intensified earthquake is limited. In addition to calculation and modification of the capacity-deformation curves of the links, four different damage states are considered for the links, according to Figure 4. As it is evident in this figure, the stresses in the wings are always less than those in web of the links. This observation is firmly grounded in the accuracy of nonlinear modelling of vertical links and the assumption of shear yielding.

In order to include strength and stiffness loss of vertical links due to the damages induced by the mainshock event, two-stage cyclic loadings are applied to the developed numerical models. In the first stage, the link is subjected to a cyclic loading until reaching a given shear strain and then the loading is stopped. In the next stage of loading, full cyclic loading is performed on the link which has already experienced some damages in the first stage. Then, the hysteresis curve of the second stage is idealized as a multi-linear curve. Figure 6 shows the schematic view of the response curves for different limit states of the link as identified in Figure 4. As it is evident, by using this approach the effects of strength and stiffness loss can be included in the capacity curves of the links. In this study, the maximum shear strains in the links are determined by applying the mainshock to the structures, and then the above-mentioned approach is adopted to modify the behaviour curves of the links.

The vertical links are modelled in PERFORM-3D® using linear “column” elements with concentrated “shear hinges-plastic strain type”. Table 3 summarises the periods and the effective translational mass participation factors of the frames for the first two vibration modes. It can be noted that the small length of the vertical link elements used in the considered frames provided higher lateral stiffness (i.e. lower fundamental period) compared to typical eccentrically braced steel frames. It should be noted that the effects of low cycle fatigue are considered in this study by taking into account the strength and stiffness degradation of the link elements under cyclic loading using different shear strains (see Figure 6). However, more accurate path dependent damage models (such as the one proposed by Benavent-Climent 2007) can be also used to simulate the response of these systems under earthquake sequences.

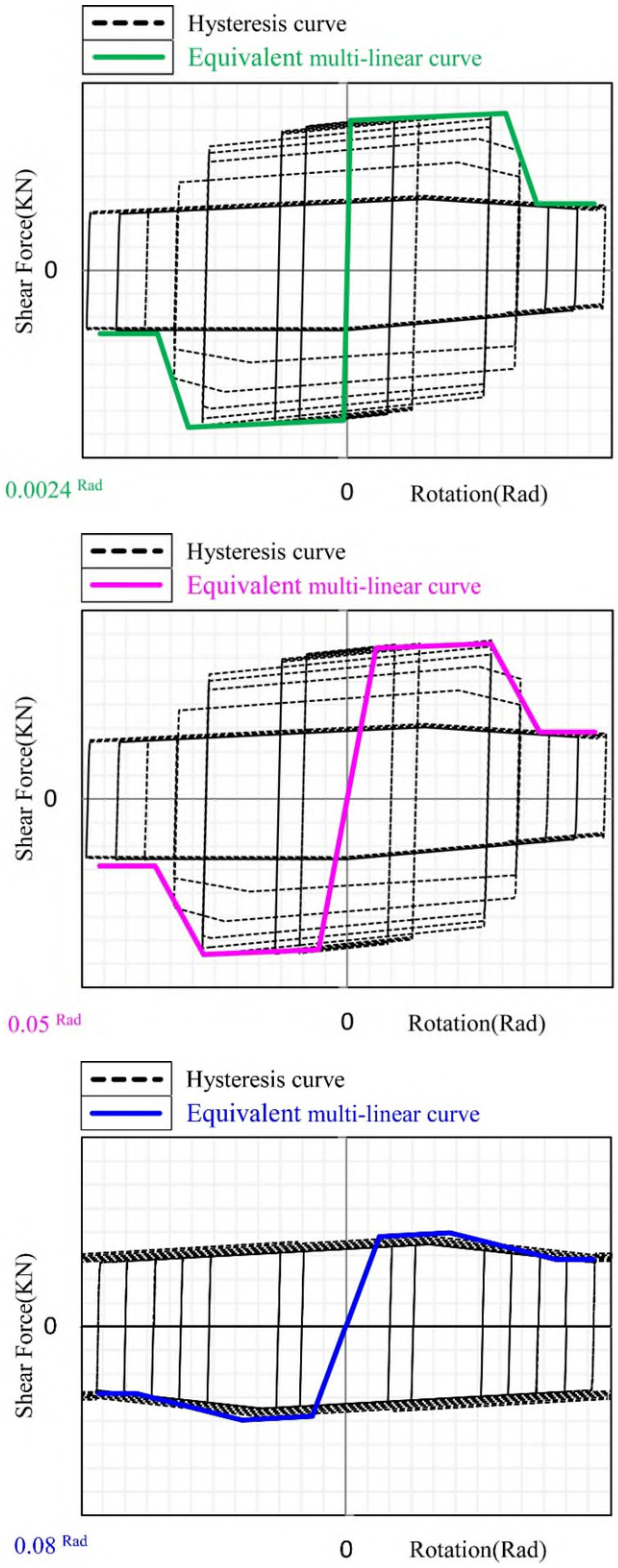

Figure 6. Schematic view of the modified capacity curves of vertical links after experiencing different shear strains

Table 3. Periods and effective translational mass participation factors for the first two vibration modes

Mode	4 storey		8 storey		12 storey	
	T(s)	M (%)	T(s)	M (%)	T(s)	M (%)
1	0.175	83.70	0.339	73.0	0.646	63.5
2	0.065	12.98	0.121	18.8	0.204	24.1

3. Proposed method for analysis of structures subjected to shocks and aftershocks

The proposed method uses incremental dynamic analyses (IDA) to apply aftershocks. Initially, a set of records is selected for the site considering local conditions and seismicity. Subsequently, the main earthquake is selected based on a specific hazard level at the site, or on a specific performance level of the structure. This implies that the main earthquake is consistent with a constant hazard level (e.g. the design hazard level of the code (step 1 in Figure 7), or has a magnitude that takes the building to a certain performance level (e.g. a Life Safety performance level (step 2 in Figure 7). The main earthquake is then applied to the structure to produce damage. As shown in Figure 7, the damaged structure is finally subjected to IDA using the selected set of records. The method is especially suitable to assess the residual capacity of the structure after applying the earthquakes. The following sections demonstrate the method through the analysis of the buildings described in section 2.

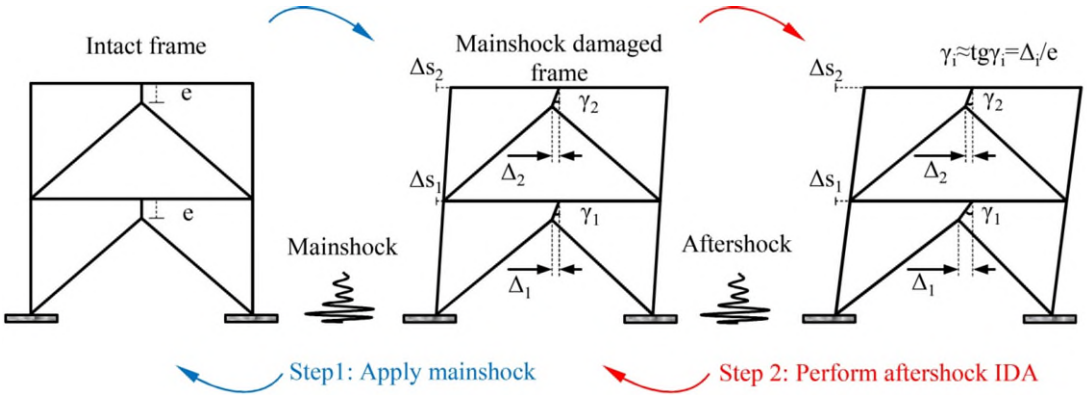

Figure 7. Proposed method for analysis of structures subjected to shocks and aftershocks (schematic)

3.1. Selection of record set and main earthquake

In this study, twelve far-fault records of soil type “C” (ASCE/SEI 41-17 classification) from the PEER database are selected for IDA and time history analyses (see main components in Table 4). The components shown in the table are selected based on the larger spectral values within the range of vibrational frequency. A design based earthquake (DBE) with a peak ground acceleration (PGA) of 0.35g and a return period of 475 years (according to the Iranian Standard No. 2800 (2014)) is selected as the main earthquake. Subsequently, all records are scaled to the maximum design hazard level of the Iranian Standard No. 2800 (2014), thus ensuring that the maximum acceleration in the record has the same value as that of the DBE. Therefore, theses earthquake records can be considered as representatives of the selected design spectrum. The frames described in section 2 are then subjected to the scaled records.

Table 4. Selected records for IDA and time history analyses

Records	Earthquake& Year	Station	R[a](km)	Component	M_w	PGA(g)
R_1	Cape Mendocino, 1992	Eureka – Myrtle & West	41.97	90	7.1	0.178
R_2	Northridge, 1994	Hollywood – Willoughby Ave	23.07	180	6.7	0.245
R_3	Northridge, 1994	Lake Hughes #4B - Camp Mend	31.69	90	6.7	0.063
R_4	Cape Mendocino, 1992	Fortuna – Fortuna Blvd	19.95	0	7.1	0.116
R_5	Northridge, 1994	Big Tujunga, Angeles Nat F	19.74	352	6.7	0.245
R_6	Landers, 1992	Barstow	34.86	90	7.4	0.135
R_7	San Fernando, 1971	Pasadena – CIT Athenaeum	25.47	90	6.6	0.110
R_8	Hector Mine, 1999	Hector	11.66	90	7.1	0.337
R_9	Kobe, 1995	Nishi-Akashi	8.70	0	6.9	0.509
R_{10}	Kocaeli, 1999	Arcelik	53.7	0	7.5	0.219
R_{11}	Chi Chi, 1999	TCU045	77.5	90	7.6	0.512
R_{12}	Friuli, 1976	Tolmezzo	15.82	0	6.5	0.417

[a] Closest distance to fault rupture

Figures 8 (a-c) compare the maximum shear strains in the links of the 4, 8 and 12 storey buildings subjected to the scaled records. Likewise, Figures 8 (d-f) compare the corresponding permanent shear strains in the links. In this study, the magnitude of the shear strain is used as an indicator of the energy dissipation capacity of the links. The results in Figure 8 show that the vertical links at the design hazard level reach yielding. The permanent strains in the links at the ground floor level of the 4, 8 and 12-storey buildings are 0.0085, 0.113 and 0.022 radians, respectively. The results confirm that the maximum strains and permanent strain in the vertical links increase with the building height.

Drifts provide an insight into the global behaviour of the buildings. Figures 9(a-c) compare the maximum inter-storey drifts (ISD) over the building height, whilst Figures 9(d-f) compare the permanent drifts. The results show that the ISD is lower than the limit set in the Iranian code (0.02 for structures with more than 5 storeys, and 0.025 for buildings lower than 5 storeys). The maximum permanent drifts of the frames under critical records generally occur at the first floor and reach 0.056%, 0.17% and 0.14% for the 4, 8 and 12 storey buildings, correspondingly (see Figure 9). Overall, the results in Figures 8 and 9 indicate that the three model buildings can sustain subsequent aftershocks.

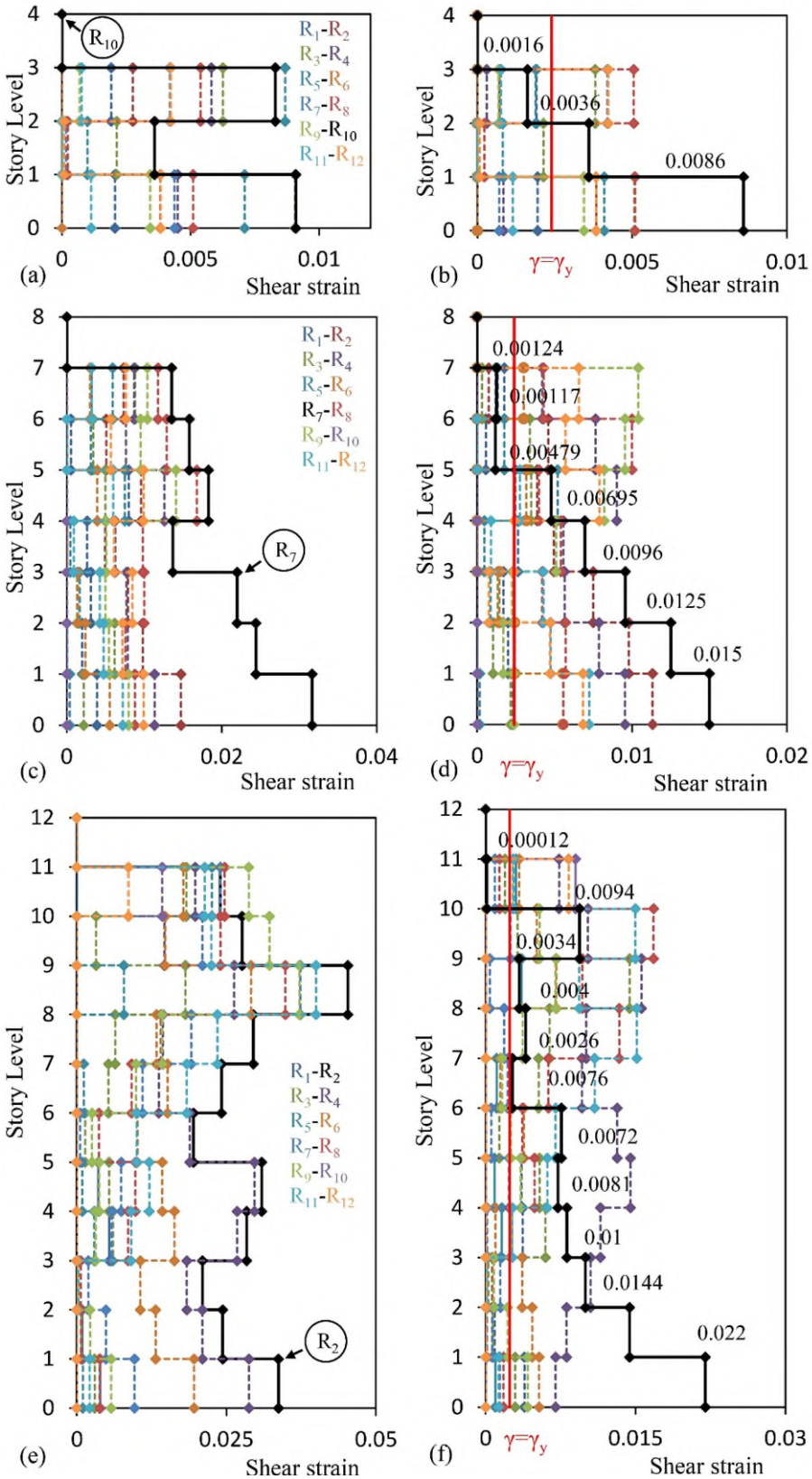

Figure 8. Maximum shear strain (a, c and e) and permanent shear strain (b, d and f) in vertical links for scaled records

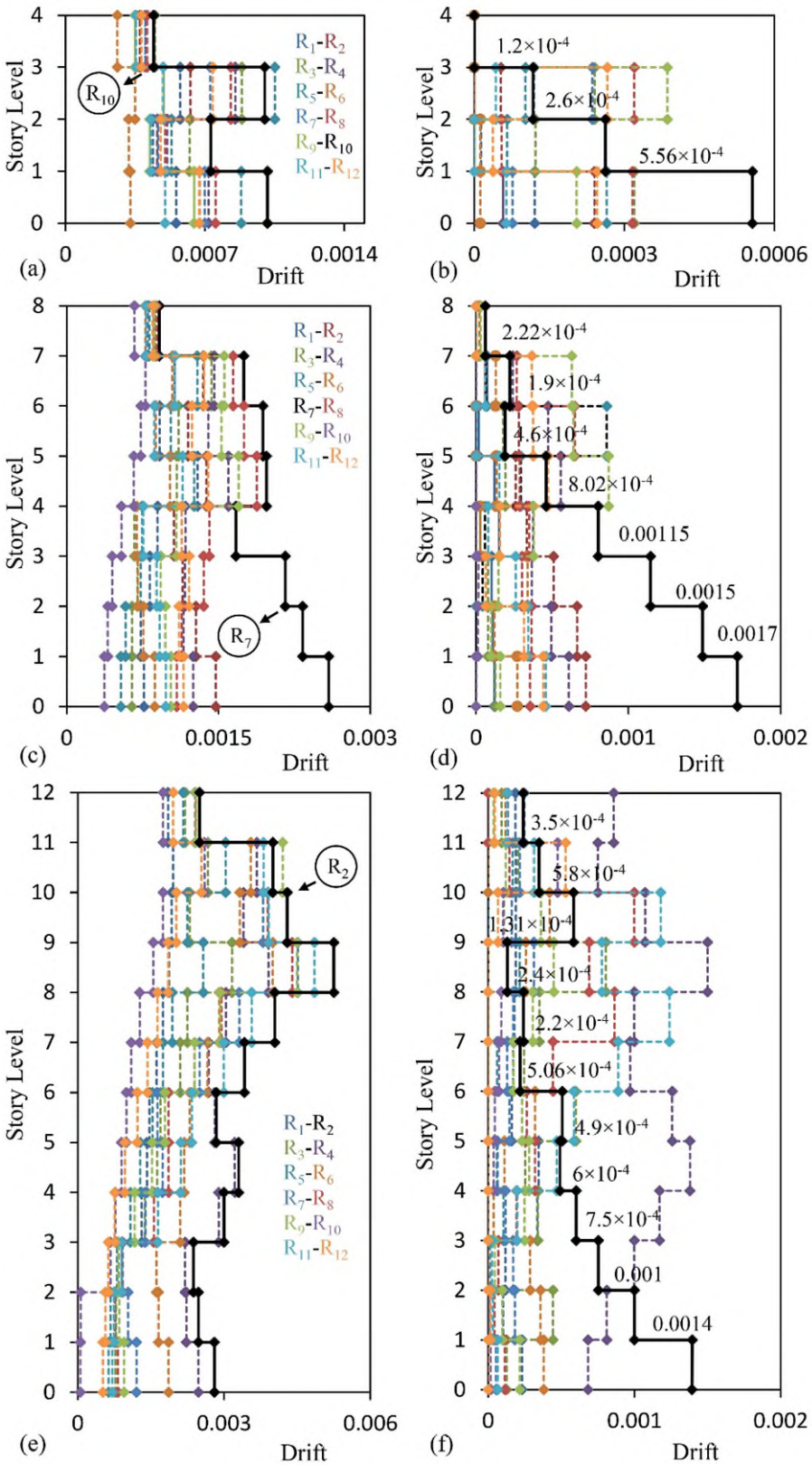

Figure 9. Maximum drift (a, c and e) and permanent drift (b, d and f) of the storeys under records scaled to the design earthquake

In this study, the records leading to the largest storey drifts and residual strain in the vertical links are taken as the main earthquake for analyses. While from the statistical point of view some of the results may divert from the average of the other responses, they should be considered in the design process to prevent undesirable failure modes. Accordingly, record R_{10} is chosen for the analysis of the 4-storey frame, R_7 for the 8-storey frame and R_2 for the 12-storey frame). Figure 8 shows the amount of energy absorbed by the links as a percentage of the total input energy to the frame after subjecting the frames to the above-mentioned records. It is shown that under any record at the design hazard level, the input energy in the frame is mainly dissipated by the vertical links, thus confirming that the vertical links work as "fuses". This also confirms than the beams, bracing and columns of the buildings remain elastic, as initially assumed in the modelling. The results of the analyses indicate the acceptable performance of the system under the DBE of Standard No. 2800 (2014). It should be noted that the results in Figure 10 are for the critical earthquake record and the percentage of the energy absorbed at different storey levels can change based on the frequency content of the input earthquake.

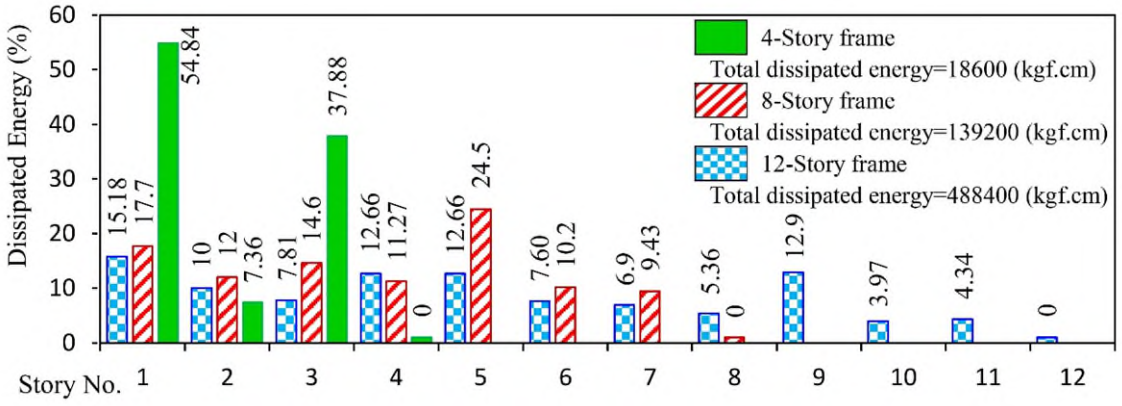

Figure 10. Energy absorbed by links at each floor under critical records

The results in Figures 9 and 10 indicate that the designed frames did not exhibit a uniform distribution of inter-storey drift and energy dissipation at different storey levels. This indicates that the adopted design methodology (based on ASCE/SEI 41-17) does not necessarily lead to optimum design solutions. It should be noted that different optimisation methods such as Uniform Damage Distribution (Moghaddam & Hajirasouliha, 2008; Nabid et al. 2018), Genetic Algorithm (Nabid et al. 2018) and Particle Swarm Optimization (Mohammadi et al. 2019) can be used to obtain the best distribution of strength and stiffness of the link elements to achieve a uniform damage distribution leading to better seismic performance. This can be a topic for further investigation in future studies.

3.2. IDA of the intact frames and the frames damaged by the main earthquake

This section investigates the seismic reliability of the buildings under aftershocks of the design earthquake (return period of 475 years). Figure 11 shows that each record consists of the main earthquake, which is the same for each building (R_{10} for the 4-storey frame, R_7 for the 8-storey frame and R_2 for the 12-frame frame), and an aftershock not related to the main

earthquake and different from one record to the other. In the analysis, a gap of 10 s was assumed between mainshock and aftershock, as shown schematically in Figure 11. It should be noted that due to the low vibration amplitudes at the end of the mainshock and the inherited damping of the selected structural system, the considered gap is sufficient to bring the buildings to rest. This is consistent with the results reported by Raghunandan et al. (2015). In this research, IDA is performed on the studied frames using the twelve records in Table 4 for buildings in two conditions:

a) Building considering the main earthquake only.

b) Building considering the main earthquake and aftershocks.

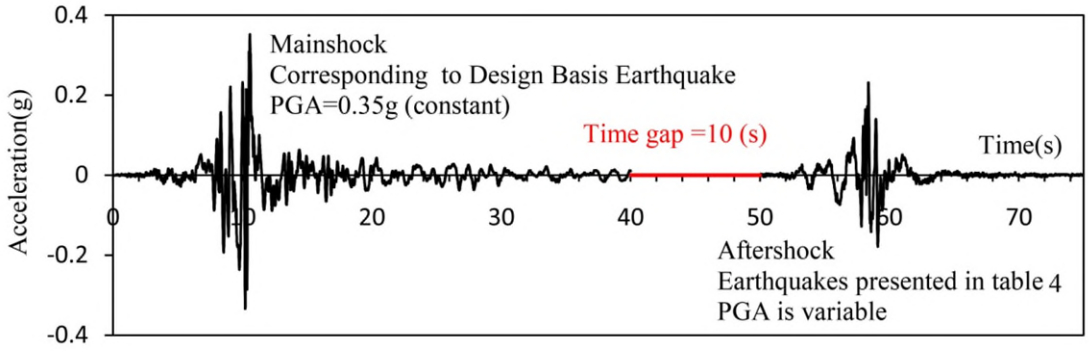

Figure 11. Main earthquake and aftershock used for IDA

In this study, the peak ground acceleration (PGA) is selected as the intensity measure, whereas the maximum shear strain in the links is selected as the response measure. For better comparison, Figures 12 to 14 compare IDA curves of the buildings in terms of PGA and strain in the links for conditions a and b.

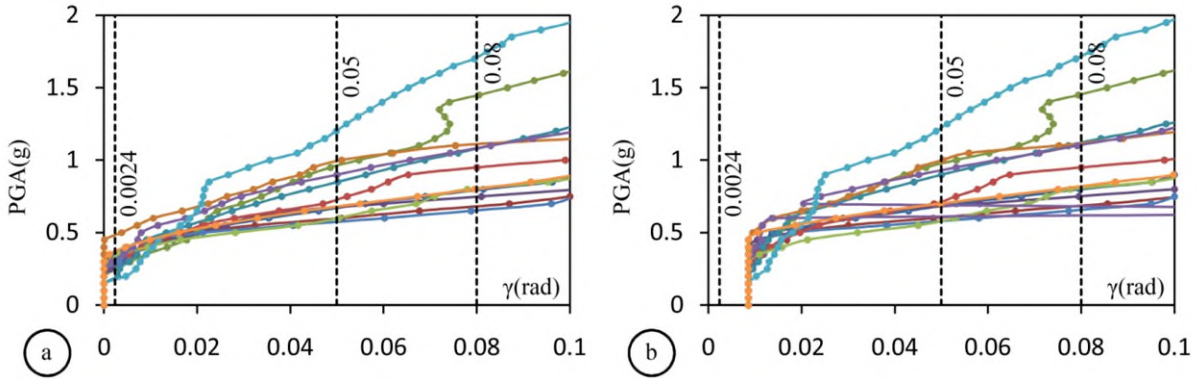

Figure 12. IDA Curves PGA vs strains in vertical links for 4-storey building (a) Condition a, (b) – Condition b

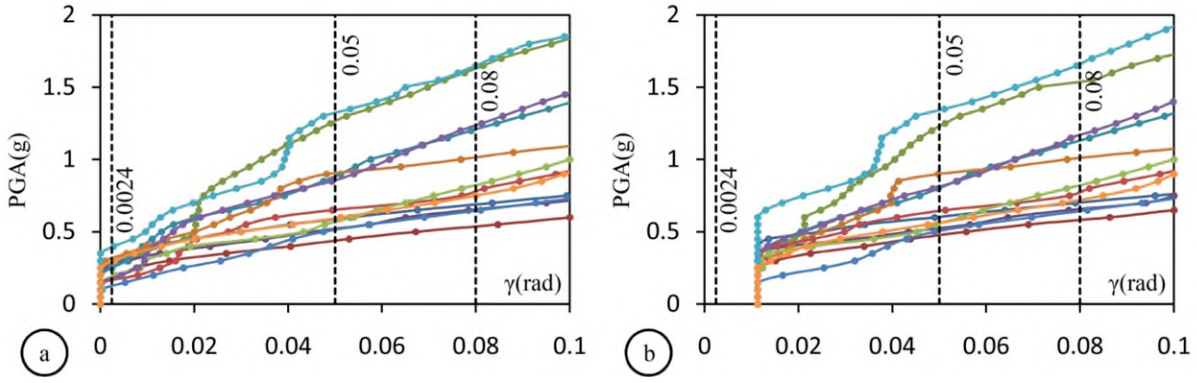

Figure 13. Curves derived from incremental dynamic analysis and damage levels for vertical links (8-frame frame) (a) - Intact frame (b) - Damaged frame due to design earthquake

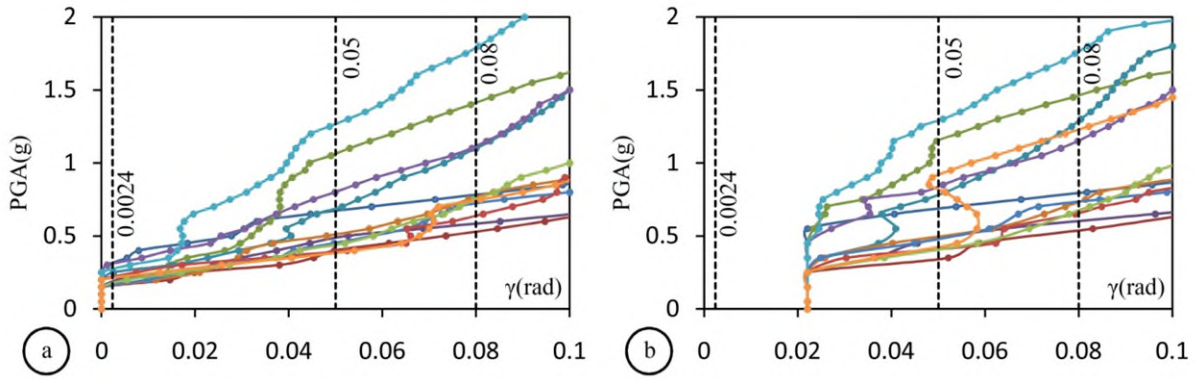

Figure 14. Curves derived from incremental dynamic analysis and damage levels for vertical links (12-frame frame) (a) - Intact frame (b) - Damaged frame due to design earthquake

Table 5 compares the level of shaking required to achieve different performance levels in the vertical links as shown in Figure 4. The results in Table 5 show that the vertical links in condition (a) yielded at intensities below the intensity corresponding to the design hazard level (i.e. DBE=0.35g). As the height of the frame increases, this intensity also decreases. This implies that shorter frames in general exhibit higher levels of reliability. The results in the table also show that the level of shaking corresponding to the desired strain levels in conditions (a) and (b) is similar (i.e. 0.05 and 0.08). This suggests that the occurrence of the design earthquake does not have a significant effect on the intensity corresponding to the different damage levels of the links. Also, it can be noted from Table 5 that the intensity corresponding to different performance levels in the links of each damaged frame under the design earthquake is several times larger than the acceleration of the design earthquake (more than 2.6 times for strain of 0.08 radians and more than 1.7 times for the strain of 0.05 radians). These observations indicate the high capacity of eccentric braced frames equipped with vertical links under high intensity levels and the probable subsequent aftershocks in seismic areas, leading to higher reliability in shorter frames.

Table 5. Medium intensity required to achieve different performance levels in vertical links (units: g)

Condition a)			
Shear strain(rad)	0.0024	0.05	0.08
4 storey frame	0.30	0.78	0.98
8 storey frame	0.24	0.76	0.96
12 storey frame	0.22	0.63	0.91
Condition b)			
Shear strain(rad)	0.0024	0.05	0.08
4 storey frame	*	0.75	0.99
8 storey frame	*	0.72	0.95
12 storey frame	*	0.60	0.92

4. Fragility curves

This section evaluates the seismic reliability of the links using a probabilistic approach. For this purpose, the collapse based on the seismic intensity parameter (IM-based) method is considered (Zareian et al., 2010). In this method, the probability of reaching the given performance level for different earthquake intensities is calculated. Accordingly, the selected seismic intensity parameter is linked to the damage state of structure, and fragility curves are developed for a given performance (damage) level. For the case study buildings, the maximum shear deformation of the links is selected as response, whereas the strain limit states defined in Figure 4 (0.05 and 0.08 radians) are considered as damage criterion. The process for developing fragility curves in this method is described in Appendix A.

Figures 15 to 17 compare the fragility curves for the examined building models. Appendix A describes the methodology used to develop these fragility curves in details. The results show that there is a close agreement between the fragility curves for two undamaged and damaged frames. This can be attributed to the fact that due to the limited damage produced by the design earthquake (main excitation), residual strains are negligible and therefore the building strength does not degrade.

In the 4-storey frame (damaged or undamaged) under a maximum acceleration of 0.35g (equivalent to the acceleration of the design earthquake), the probability of reaching a shear strain of 0.05 rad in the vertical links is negligible. In the 8 and 12 storey frames (damaged or undamaged), this probability is estimated to be less than 2.5 and 12 percent, respectively. In the examined damaged frames, it is expected that, under aftershocks with intensities higher than 0.35g, the strain in the links will not exceed the specified values. This is an indication of the high safety of the links in areas with high seismic hazard. These results confirm that the proposed system with links provides high seismic reliability under the design earthquake and its aftershock.

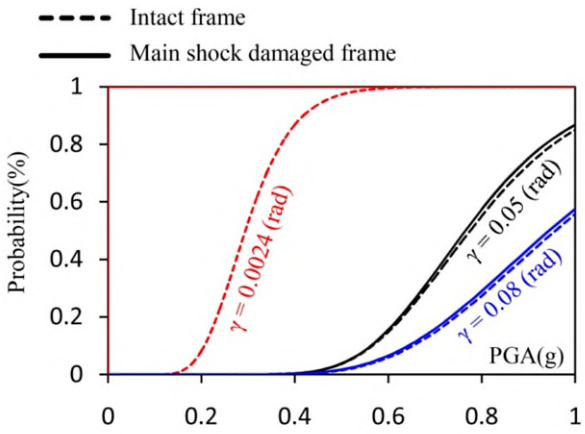

Figure 15. Fragility curves for various limit states of the vertical links (4-storey frame)

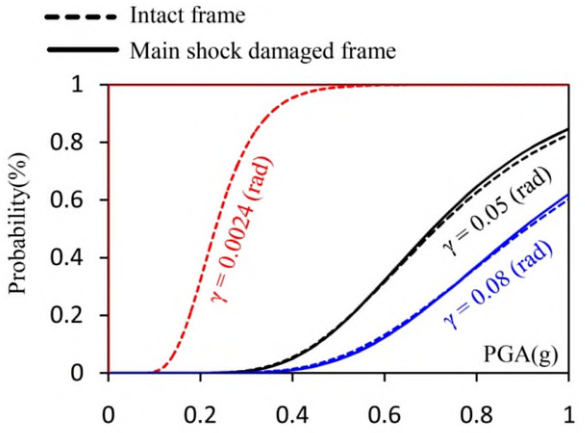

Figure 16. Fragility curves for various limit states of the vertical links (8-storey frame)

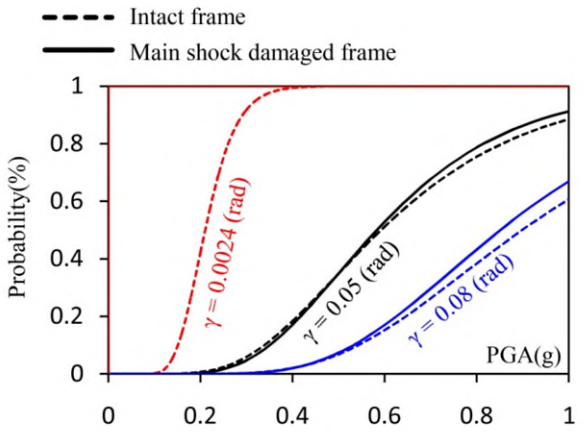

Figure 17. Fragility curves for various limit states of the vertical links (12-storey frame)

5. Simplified (approximate) method

Whilst the methodology described in Section 4 is expected to provide reliable results, the application of IDA may be rather time-consuming for use in practical assessment of a large number of buildings under a set of mainshock and aftershock earthquake records. Consequently,

in this section a simplified method is adopted based on widely used pushover analyses. In this method, the original earthquake corresponding to the required hazard level (or performance level) is initially applied to the building (Figure 18). Subsequently, a pushover analysis is performed on the damaged building assuming a lateral load distribution proportional to the shape of the first vibration mode. It should be noted that for the studied frames the period of the first translational mode of the damaged frames is below 1.0 s with the effective mass coefficient close to or greater than 75% (see Table 3).

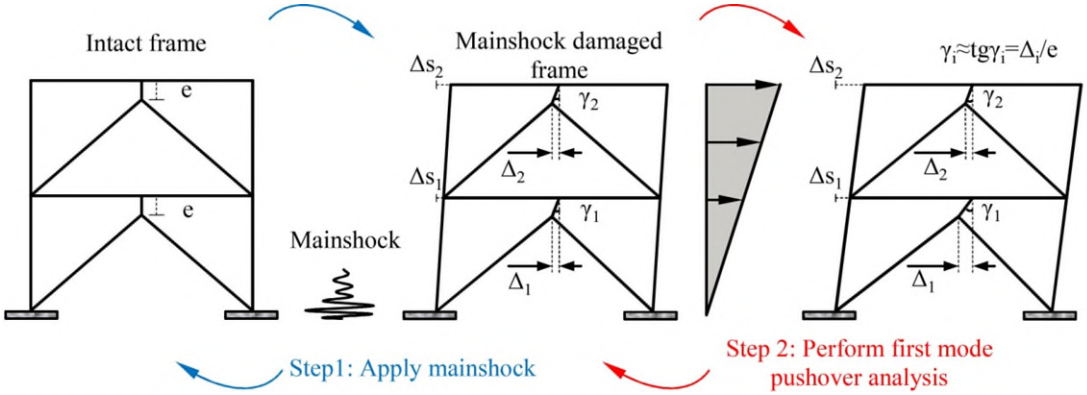

Figure 18. Procedure to obtain capacity curve of the damaged building based on the pushover analysis (schematic)

The direction of analysis is chosen so as to increase the structural deformation of the elements, as well as the permanent displacements of the frames. The drop in strength and stiffness can be estimated by comparing the capacity curve of the 'undamaged' and 'damaged' frames due to the main earthquake. Moreover, if the capacity curve is plotted using the spectral accelerations and displacements (ADRS), the spectral acceleration for any limit state of the building can be estimated.

5.1. Selection of main earthquake

The main earthquake is chosen in the same way as in section 3.1. Accordingly, from scaled records, the excitation that produces the larger displacement and residual strains were selected as main earthquakes (see Figures 8 and 9). Thus, after being scaled to the hazard level of the design earthquake based on Standard No. 2800 (2014), records R_{10}, R_7 and R_2 were applied to the 4, 8 and 12 storey frames as the main earthquake, respectively.

5.2. Pushover analysis - main earthquake

To investigate the impact of the main earthquake on the stiffness and lateral strength of the frames, pushover curves are obtained for two conditions:

i) ***Undamaged frames*** pushed using a modal pattern load distribution. The average roof drift ratio (roof displacement divided by the total height of the frame) is then recorded at shear strains of 0.05, 0.08, and 0.1 radian the links, as well as at the onset of yielding in the storey beams of the braced spans.

ii) ***Damaged frames***, i.e. the pushover is carried out after applying the main earthquake.

Figure 19 compares the capacity curves of the undamaged and damaged frames. Drift ratios at different damage levels in the undamaged frames are also illustrated. It is shown that the first failures are related to the yielding in the vertical shear panels, and the links in the lower storeys experience the highest shear strain. The results in Figure 19 indicate that, as expected, the elastic lateral stiffness (k) of the frames decreases with an increase in height. It can be also noted that the capacity curves of the frames in both damaged and undamaged states do not exhibit an abrupt loss of strength and stiffness degradation, which is usually caused by the brace's buckling. This observation validates the assumption that the force in the braces remains constant after yielding of the vertical links. It also proves that the vertical links can efficiently act as a seismic fuse dissipating energy system.

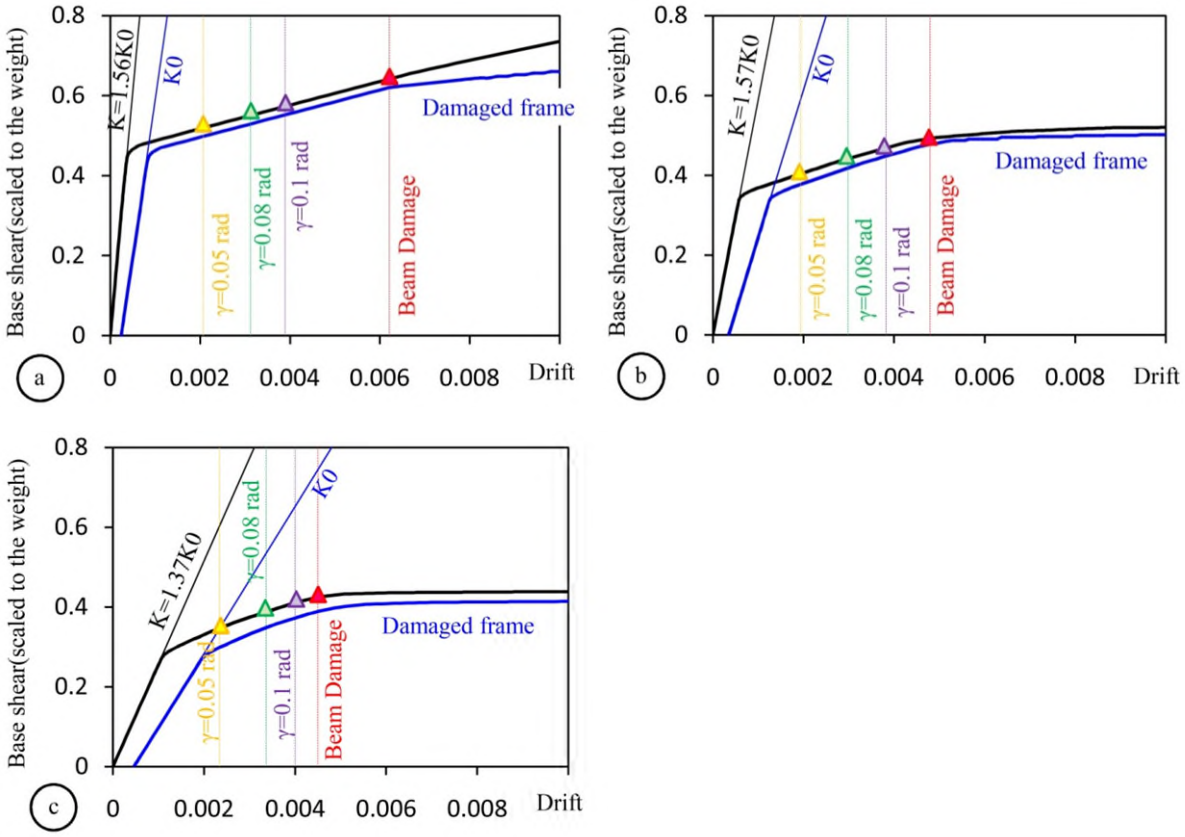

Figure 19. Capacity curves of undamaged and damaged frames and limit states corresponding to different damage levels in the elements: a) 4-storey, b) 8-storey, and c) 12-storey frames

The results also show that the application of the design earthquake does not reduce significantly the stiffness and strength of the model frames. The average permanent drifts for the 4, 8, and 12 storey frames under the design earthquake are 0.024, 0.035 and 0.046%, respectively. Note that the overall loss of strength is less than 10%, whilst the strength reduces more significantly as the building height increases.

As mentioned before, the damaged frame was loaded in a direction that would increase the deformations and permanent displacements. In the IDA, the effect of some of the records of the

damaged frame can have an opposite effect, thus reducing the deformation and residual strain. Accordingly, the results of the two methods will be different. As such, the main advantage of the proposed method based on pushover analysis is to significantly reduce the computational time required to assess the residual capacity of complex buildings under sequential earthquakes. However, more analyses may be required to investigate the efficiency of the proposed methodology for tall buildings, where the effect of higher modes can be dominant, and near field earthquakes including the directivity effects.

6 Summary and conclusions

Based on the outcomes of this study, the following conclusions can be drawn:

- In addition to the intensity of the applied excitation, the displacement and deformation responses of the frames are also sensitive to the frequency content of the input earthquake record. Under the 2800 code representative records (return period of 475 years) as the main earthquake event, the maximum and permanent deformation demands in the vertical links are both negligible (less than 0.05 radians). This indicates that these elements in all of the studied frames perform in the high performance levels. The maximum and permanent storey drift demands exhibited by the considered frames are also considerably lower than the permissible code values (2.5% for less than 5 storey frames and 2% for more than 5 storey frames).
- Almost all of the earthquake energy applied to the frames is absorbed and dissipated by the vertical links. Accordingly, in the frames with the vertical links the assumptions of elastic behaviour of the other structural elements (beams, columns, and braces) and the fuse role of the shear panels are valid.
- Application of the design earthquake in frames does not have a significant effect on the intensity corresponding to the different damage levels of the vertical links. The required intensity to provide higher performance level in the vertical links is much higher than the intensity of the design earthquake of 2800 code. The intensities which are corresponding to the strain of 0.08 and 0.05 radians are estimated to be more than 2.6 and 1.7 times the magnitude of the design earthquake, respectively.
- Although in the event of successive earthquakes the systems with vertical fuse links have high seismic reliability, for a certain level of intensity or damage level, an increase in the height of the frame decreases the reliability level.
- By comparing the fragility curves, no noticeable difference was evident between various damage levels of the undamaged and the damaged frames. In the 4-storey frame (undamaged or damaged) under the excitation with a maximum acceleration of 0.35 g (equivalent to the acceleration of the design earthquake) the probability that the maximum shear strain of the vertical links reaches the 0.05 radian threshold is almost zero. In the 8 and 12-storey frames (undamaged or damaged) this probability is estimated to be less than 2.5 and 12 percent, correspondingly.

- The energy absorbing fuses of the frames remain in the high performance levels, even under relatively strong aftershocks. This demonstrates the high seismic resistance and sufficient safety of this system under the main earthquake and possible aftershocks in the areas with high seismic hazard.
- After application of the design earthquake and therefore development of the permanent displacements and deformations, the frames still have high capacity and strength. For each damage level, there is no significant difference between the corresponding spectral acceleration values in the undamaged and damaged frames. However, the value of this parameter in the damaged frame is always lower. As the frame height increases, in general, the amount of the permanent displacements and the loss of the frame strength after the main earthquake event increase.

References

ABAQUS, Version 6.14 (2014), *ABAQUS User Manual*, SIMULIA World Headquarters. Rissing Sun Mills 166 Valley Street, Providence (RI 02909-2499, USA).

Abdollahzadeh, G., Mohammadgholipour, A. and Omranian, E. (2019) "Development of the Performance-Based Plastic Design Method by Considering the Effects of Aftershocks", *Journal of Earthquake Engineering*, DOI: 10.1080/13632469.2019.1692739.

Aghlara, R. and Tahir, M.M. (2018) "A passive metallic damper with replaceable steel bar components for earthquake protection of structures", *Engineering structures*, 159, 185-197.

ASCE/SEI Standard 41-17 (2017), *Seismic Evaluation and Retrofit of Existing Buildings American Society of Civil Engineers*, Reston, Virginia, USA.

Benavent-Climent, A. (2007) "An energy-based damage model for seismic response of steel structures", *Earthquake Engineering & Structural Dynamics*; 36(8):1049-1064.

Bouwkamp J, Vetr MG and Ghamari A (2016) "An analytical model for inelastic cyclic response of eccentrically braced frame with vertical shear link (V-EBF)", *Case Studies in Structural Engineering*, 6: 31-44.

Burton H, Sreekumar S, Sharma M and Sun H (2017) "Estimating aftershock collapse vulnerability using mainshock intensity, structural response and physical damage indicators," *Structural Safety*, 68:85–96.

Computers and Structures Inc., CSI (2015), *Structural and Earthquake Engineering Software, ETABS, Extended Three Dimensional Analysis of Building Systems Nonlinear*, Version 15.2.2, Berkeley, CA, USA.

Computers and Structures Inc., CSI (2016), *Structural and Earthquake Engineering Software, PERFORM-3D Nonlinear Analysis and Performance Assessment for 3-D Structures*, Version 6.0.0, Berkeley, CA, USA.

Della Corte G, D'Aniello M and Landolfo R (2013) "Analytical and numerical study of plastic overstrength of shear links," *Journal of Constructional Steel Research*, 82:19–32.

Fragiacomo M, Amadio C and Macorini L (2004) "Seismic response of steel frames under repeated earthquake ground motions," *Engineering Structures*, 26: 2021-2035.

Ghobarah A and Elfath HA (2001) “Rehabilitation of a reinforced concrete frame using eccentric steel bracing,” *Engineering Structures*, 23(7): 745-55.

Guerrero H, Ruiz-García J, Escobar JA and Terán-Gilmore A (2017) “Response to seismic sequences of short-period structures equipped with Buckling-Restrained Braces located on the lakebed zone of Mexico City,” *Journal of Constructional Steel Research*, 137: 37-51.

Hatzigeorgiou GD and Beskos DE (2009) “Inelastic Displacement Ratios for SDOF Structures Subjected to Repeated Earthquakes,” *Engineering Structures*, 31: 2744–2755.

Hatzigeorgiou GD and Liolios AA (2010) “Nonlinear Behaviour of RC Frames Under Repeated Strong Ground Motions,” *Soil Dynamics and Earthquake Engineering*, 30: 1010–1025.

Institute of National Building Regulations (2008), *Design and construction of Steel Structures*, Topic.10, Ministry of Roads & Urban Development, Iran.

International Institute of Earthquake Engineering and Seismology (IIEES), Web Site:

International Institute of Earthquake Engineering and Seismology, http://www.iiees.ac.ir; Accessed: July 2019.

Jeon JS, DesRoches R, Lowes LN and Brilakis I (2015) “Framework of aftershock fragility assessment-case studies: Older California reinforced concrete building frames,” *Earthquake Engineering & Structural Dynamics*, 44(15) :2617-2636.

Jia, L.J., Xie, J.Y., Wang, Z., Kondo, K. and Ge, H. (2020) “Initial studies on brace-type shear fuses”, *Engineering Structures*, 208, 110318.

Khatami, M., Gerami, M., Kheyroddin, A. and Siahpolo, N. (2019) “The effect of the mainshock-aftershock on the estimation of the separation gap of regular and irregular adjacent structures with the soft story”, *Journal of Earthquake and Tsunami*, DOI: 10.1142/S1793431120500086.

Lee K and Foutch DA (2004) “Performance Evaluation of Damaged Steel Frame Buildings Subjected to Seismic Loads,” *Journal of Structural Engineering*, 130(4): 588-599.

Li Q and Ellingwood BR (2007) “Performance evaluation and damage assessment of steel frame buildings under main shock-aftershock sequences,” *Earthquake Engineering and Structural Dynamics*, 36: 405-427.

Li Y, Song R and Van De Lindt J (2014) “Collapse Fragility of Steel Structures Subjected to Earthquake Mainshock-Aftershock Sequences,” *Journal of Structural Engineering*; 140(12): 1-10.

Loulelis D, Hatzigeorgiou GD and Beskos DE (2012) “Moment resisting steel frames under repeated earthquakes,” *Earthquake and Structures*, 3(3-4): 231-248.

Luco N, Bazzurro P and Cornell CA (2004) “Dynamic versus static computation of the residual capacity of mainshock-damaged building to withstand an aftershock,” In: Proceedings 13th. World Conference on Earthquake Engineering, Paper No. 2405, Vancouver.

Mazzolani FM, Corte GD and D'Aniello M (2009) “Experimental analysis of steel dissipative bracing systems for seismic upgrading,” *Journal of Civil Engineering and Management*, 15(1): 7-19.

Moghaddam, H., Hajirasouliha I (2008) “Optimum strength distribution for seismic design of tall buildings”. *Structural Design of Tall and Special Buildings*, 17(2), 331-349.

Mohammadi, R.K, Garoosi, M.R. and Hajirasouliha, I. (2019) "Practical method for optimal rehabilitation of steel frame buildings using buckling restrained brace dampers". *Soil Dynamics and Earthquake Engineering*, 123, 242-251.

Mohsenian V and Mortezaei A. (2018) "Evaluation of seismic reliability and multi level response reduction factor (R factor) for eccentric braced frames with vertical links," *Earthquakes and Structures*; 14(6): 537-549.

Mohsenian V., Filizadeh R., Ozdemir Z. Hajirasouliha I (2020) "Seismic performance evaluation of deficient steel moment-resisting frames retrofitted by vertical link elements", *Structures*, 26: 724-736.

Mohsenian V., Mortezaei A. (2019) "A new energy-absorbing system for seismic retrofitting of frame structures with slender braces", *Bulletin of Earthquake Engineering*, 17: 2715-2739.

Nabid, N., Hajirasouliha, I. and Petkovski, M. (2018) "Performance-based optimisation of RC frames with friction wall dampers using a low-cost optimisation method. *Bulletin of Earthquake Engineering*, 16(10), 5017-5040.

Nabid, N., Hajirasouliha, I. and Petkovski, M. (2019) "Adaptive low computational cost optimisation method for performance-based seismic design of friction dampers", *Engineering Structures*, 198, 109549.

Parekar, S.D. and Datta, D. (2020) "Seismic behaviour of stiffness irregular steel frames under mainshock-aftershock", *Asian Journal of Civil Engineering*, 21: 857-870.

Park, S.W., Park, H.S., Oh, B.K. and Choi, S.W. (2018) "Fragility Assessment Model of Building Structures Using Characteristics of Artificial Aftershock Motions", *Computer-Aided Civil and Infrastructure Engineering*, 33(8): 691-708.

PEER Ground Motion Database, Pacific Earthquake Engineering Research Center, Web Site: http://peer.berkeley.edu/peer-ground-motion-database; Accessed: Jan 2019.

Permanent Committee for Revising the Standard 2800 (2014); Iranian Code of Practice for Seismic Resistant Design of Buildings, 4th Edition, Building and Housing Research Center, Tehran, Iran.

Qu, B., Liu, X., Hou, H., Qiu, C. and Hu, D. (2018) "Testing of buckling-restrained braces with replaceable steel angle fuses", *Journal of Structural Engineering*, 144(3), 04018001.

Rad, A.A., Hazaveh, N.K., MacRae, G.A., Rodgers, G.W. and Ma, Q. (2019) "Structural straightening with tension braces using aftershocks–Shaking table study", *Soil Dynamics and Earthquake Engineering*, 123: 399-412.

Raghunandan M, Liel AB and Luco N (2015) "Aftershock collapse vulnerability assessment of reinforced concrete frame structures," *Earthquake Engineering and Structural Dynamics*, 44(3): 419-439.

Ruiz-García J (2012) "Mainshock-aftershock ground motion features and their influence in building's seismic response," *Journal of Earthquake Engineering*, 16(5): 719-737.

Ruiz-García J and Aguilar JD (2015) "Aftershock seismic assessment taking into account post-mainshock residual drifts," *Earthquake Engineering and Structural Dynamics*, 44(9): 1391–1407.

Ruiz-García J and Aguilar JD (2017) "Influence of modeling assumptions and aftershock hazard

level in the seismic response of post-mainshock steel framed buildings," *Engineering Structures*, 140: 437–446.

Ruiz-García J and Negrete-Manriquez JC (2011) "Evaluation of drift demands in existing steel frames under as-recorded far-field and near-fault mainshock-aftershock seismic sequences," *Engineering Structures*, 33: 621-634.

Ruiz-García J, Bojórquez E and Corona E (2018a) "Seismic behavior of steel eccentrically braced frames under soft-soil seismic sequences," *Soil Dynamics and Earthquake Engineering*, 115: 119–128.

Ruiz-García J, Yaghmaei-Sabegh S and Bojórquez E (2018b) "Three-dimensional response of steel moment-resisting buildings under seismic sequences," *Engineering Structures*, 175: 399-414.

Sabouri-Ghomi S and Saadati B (2014) "Numerical Modeling of Links Behavior in Eccentric Bracings with Dual Vertical Links," *Numerical Methods in Civil Engineering*; 1(1):14-20.

Shi, F., Saygili, G., Ozbulut, O.E. and Zhou, Y. (2020) "Risk-based mainshock-aftershock performance assessment of SMA braced steel frames", *Engineering Structures*, 212, p.110506.

Silwal, B. and Ozbulut, O.E. (2018) "Aftershock fragility assessment of steel moment frames with self-centering dampers", *Engineering Structures*, 168: 12-22.

Song R., Li Y and Van De Lindt J (2014) "Impact of Earthquake Ground Motion Characteristics on Collapse Risk of Post-Mainshock Buildings Considering Aftershocks," *Engineering Structures*, 81: 349–361.

Stratan A and Dubina D (2002) "Seismic performance of eccentric braced frames with removable low yield steel link," In: Proceedings of International Conference Earthquake Loss Estimation and Risk Reduction, Bucarest, Romania, pp. 24-26.

Sunasaka Y and Kiremidjian A (1993) "Method for Structural Safety Evaluation Under Main-Shock–After-Shock Earthquake Sequences," Report No. 105, The John A. Blume Earthquake Engineering Center, Stanford University.

Veismoradia S, Cheraghia A and Darvishanb E (2018) "Probabilistic mainshock-aftershock collapse risk assessment of buckling restrained braced frames," Soil Dynamics and Earthquake Engineering, 115: 205-216.

Vetr MG, Ghamari A and Bouwkamp J (2017) "Investigating the nonlinear behavior of eccentrically braced frame with vertical shear links (V-EBF)", Journal of Building Engineering, 10: 47-59.

Yang, T.Y., Li, T., Tobber, L. and Pan, X. (2020) "Experimental and numerical study of honeycomb structural fuses", *Engineering Structures*, 204, 109814.

Zare M (2015) "Response Quality to the Van Earthquake in Turkey of 23 October 2011, Mw7.2, for Hazards Reduction," *Environmental Hazard Management*, 1(2): 189-202

Zareian F, Krawinkler H, Ibarra L and Lignos D (2010) "Basic Concepts and Performance Measures in Prediction of Collapse of Buildings under Earthquake Ground Motions," *The Structural Design of Tall and Special Buildings*, 19: 167-181.

APPENDIX A

This section explains the details of the methodology used to develop the fragility curves shown in Figures 13 to 15. In the first step, the maximum acceleration (PGA(g)) corresponding to the predefined values of shear strain in the vertical links $\gamma_{Allowable}$ are extracted from the curves during the IDA analysis (Figures 10 to 12). In the next step, by assuming the recorded values have a log normal distribution, their probability density function (F(x)) is derived after computing the mean value (μ) and the standard deviation (δ).

According to Figure A, by replacing the value of X_0 with the given earthquake intensity, the area under the curve of the probability density function (from $-\infty$ to X_0) is the probability of exceeding the related damage level. It means that for the given intensity, the probability that the responses of the vertical links reach the considered damage level, is "*P*". It is obvious that the difference between "*P*" and 1 indicate the seismic reliability of structure. The curve that results from repeating this process for various seismic intensities is called "fragility curve" for the considered damage level.

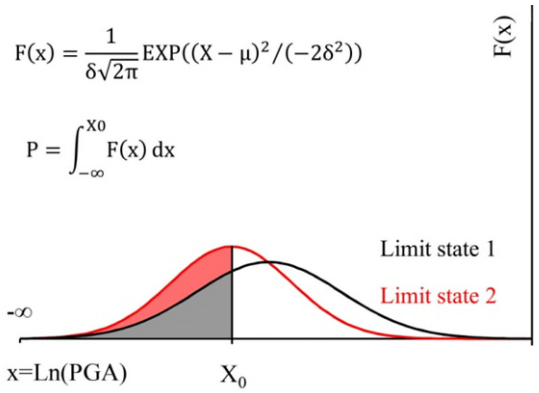

Figure A. Computation of exceedance probability for a constant performance level at a hazard level of X_0 (schematic)